fire

MDPI

Article

Safety Assessment of Hydrogen Jet Fire Scenarios within Semi-Confined Spaces

Brock Virtue, Javad Mohammadpour, Fatemeh Salehi * and Rouzbeh Abbassi

School of Engineering, Macquarie University, Sydney, NSW 2109, Australia
* Correspondence: fatemeh.salehi@mq.edu.au; Tel.: +61-(02)-9850-7303

Abstract: Hydrogen fuel cell vehicle (HFCV) technology poses great promise as an alternative to significantly reduce the environmental impact of the transport sector's emissions. However, hydrogen fuel cell technology is relatively new, therefore, confirmation of the reliability and safety analysis is still required, particularly for fire scenarios within confined spaces such as tunnels. This study applied the computational fluid dynamics (CFD) simulations in conjunction with probabilistic calculation methods to determine the associated thermal risk of a hydrogen jet fire in a tunnel and its dependency on scenarios with different tunnel slopes, longitudinal and transverse ventilation velocities, and fire positions. A large-scale model of 102 m in which the effects of outlined parameter variations on the severity of the fire incident were analysed. It is found that both tunnel ventilation techniques and slope were critical for the effective ejection of accumulated heat. With ventilation playing a primary role in the ejection of heat and gas and slope ensuring the stability of the ejected heat, probabilities of thermal burns were found to be reduced by up to approximately 35% with a strong suggestion of critical combinations to further reduce the dangers of hydrogen tunnel fires.

Keywords: computational fluid dynamics (CFD); safety assessment; hydrogen fires; tunnel safety

Citation: Virtue, B.; Mohammadpour, J.; Salehi, F.; Abbassi, R. Safety Assessment of Hydrogen Jet Fire Scenarios within Semi-Confined Spaces. *Fire* **2023**, *6*, 29. https://doi.org/10.3390/fire6010029

Academic Editors: Qiangling Duan and Depeng Kong

Received: 17 November 2022
Revised: 15 December 2022
Accepted: 9 January 2023
Published: 12 January 2023

1. Introduction

Hydrogen fuel cell vehicle (HFCV) technology may provide an excellent decarbonisation solution for the transport sector, particularly heavy-duty vehicles. The growth of hydrogens' popularity and support is now evident through the emergence of the global hydrogen community [1], and the demand for effective safety analysis and risk assessment of HFCVs is ever-growing and essential for appropriate public integration.

Analysis of accidental scenarios involving hydrogen is essential since hydrogen's characteristics and properties vary from traditional fuels [2]. Primarily, the buoyancy of hydrogen is a point of interest for the safety of the fuel, having a low density of 0.0838 kg/m^3 at normal temperature and pressure (NTP), approximately 14 times lighter than air density at 1.205 kg/m^3 presents both safety benefits and dangers related to the fuel. High buoyancy within open systems accommodates rapid dispersion and diffusion of hydrogen, in turn reducing concentrations to a safe level below the lower flammability limit (LFL) effectively [1–5]. However, within confined and semi-confined spaces such as tunnels, it poses a hazard of accumulation and/or ignition of such entrapped gas, which may present severe consequences such as flash fire or explosion. Additionally, hydrogen is highly flammable, with a wide flammability limit in air of 4 to 75% and low ignition energy of 0.02 mJ [2,6,7], presenting a requirement of building upon a database for the risk assessment of HFCV accidents, especially within tunnels when the buoyancy effect is not favourable. Hydrogen has no threshold limit value (TLV) and is not carcinogenic. However, being odourless, colourless, and tasteless, its detection through human sensory methods is extremely difficult and, in turn, raises issues when leakage occurs in confined spaces where high concentrations may accumulate undetected [5,7]. Hydrogen also burns with a colourless flame [2].

Gas release from either the pressure relief device or a small pinhole rupture may result in a highly transient jet fire if ignited, which is the focus of this study. These jet flames generated from the HFCV have the potential to be very long in flame length and have very high flame temperatures [5,8]. In terms of compressed gas vehicles, jet fires are presented as the most common fire risk, either from tank rupture or thermal pressure relief device (TPRD) ignition. Within a confined space such as a tunnel, a hydrogen jet fire poses added risk to assets and personnel involved through exposure to high-temperature flame. Hydrogen combustion also consumes a large amount of oxygen which also presents the risk of oxygen deficiency. In addition, hydrogen jet fires have a higher potential to cause burns to the human body, which is a serious determinant of the safety aspect of HFCV application [3,6,9,10].

Many studies have used computational fluid dynamics (CFD) simulations to understand the impact of hydrogen jet flame hazards within tunnels for different scenarios [6,11–13]. Gu et al. [6] adopted a large-scale CFD model to explore the effects of possible varied tunnel/situational characteristics of the location and the rate of the leakage, tunnel cross-sectional area, and longitudinal and transverse ventilation on both diffusion of the leaked hydrogen and the temperature distribution of the jet fire incident. Seike et al. [14] focused on the impact of tunnel slope on the propagation of heat and gases and found that hydrogen propagated much faster than traditional gasoline fires with a slope having a direct effect on distribution. A further study was recommended for the variation of ventilations to slope to determine a critical relationship between slope and ventilation magnitude and direction. Shibani et al. [15] captured the effects of multiple hydrogen fires within a large-scale tunnel where the effects of position and longitudinal ventilation were placed under scope, finding that increased slope raised the severity of temperature zones at the tunnel exits.

Concerning structural damages, Sandia [16] performed a risk analysis to determine what scenarios were likely to occur in the event of an accident involving HFCVs, providing a comprehensive analysis of the jet fires and possible hazards to the infrastructure and materials of the tunnel in which it was determined with ventilation, localised concrete spalling is unlikely. The temperature distribution of hydrogen jet fire was determined using CFD with results detailing effects on the structural integrity of the tunnel and/or the structural epoxy even when ventilation was deactivated [16]. Damages are likely to be caused by overpressure in explosion scenarios [5,16–18], whereas jet fires present less of a significant risk compared to an explosion.

Combined CFD with probabilistic methods have been adopted in previous studies to develop a quantitative risk analysis (QRA) for traditional buoyant systems and infrastructure [19] and can be used as a guide in developing hydrogen safety guidelines. A key challenge to conducting a reliable QRA for hydrogen is the lack of data behind gaseous hydrogen incidents. Moradi et al. [9] outlined a generalised summary of data needed to perform a QRA on hydrogen systems effectively. Notably, jet flame risk assessment and data are mentioned affirming the need for the development of large-scale experimental data for the advancement and validation of such models [9]. Additionally, the gaseous hydrogen effects of jet fires on humans are emphasised with thermal effects, oxygen deficit, and overpressure. Upon a review of studies of hydrogen accidents' impact on human life, it is evident that research behind this field is limited.

Building upon this, studies were conducted on hydrogen properties and hydrogen comparative risk to traditional fuels such as methane and LPG [2,3,7,20]. Some studies focused on the safety distance of hydrogen fire within tunnels which have been evident in terms of diffusion and temperature distribution [6,13–15]. However, the effects and risk analysis of such fires on personnel within the scenario are limited. It is concluded that hydrogen as a fuel poses a greater risk, primarily due to the increased probability of fire and explosion based on its characteristics of a wide flammability range and low ignition energy. The general requirement for risk associated with HFCV implementation should be equal to, or less than the risk of conventional fuelled [1]. Considering the risk of hydrogen

application to transport at present, it is understandable that this requirement has not yet been achieved as identified knowledge gaps are yet to be filled [9,21].

Despite previous studies, there is a lack of risk analysis for important tunnel characteristics of slope and ventilation in both transverse and longitudinal directions, with detailed study of this likely "real world" scenario of a combination of these parameters being minimal. Whilst correlation may be based upon buoyant conventional fuel scenarios [22,23], it is evident that hydrogen as fuel needs examination in these scenarios not only due to its characteristics and properties but also in determining hydrogen diffusion, temperature distribution, and oxygen consumption of the possible outcomes of hydrogen jet fire and their effects on human life which can help to develop a comprehensive risk assessment. Hence, this study aims to analyse a relationship between tunnel ventilation techniques and the tunnel slope and further enhance the understanding of the risk associated with hydrogen jet fire in confined and semi-confined environments. For this purpose, a combined CFD-probabilistic method is adopted. Results obtained in this paper are extendable and can be used in correlation to further studies, such as overpressure, to capture more details of the risk behind HFCVs. The outcome of this study would be beneficial for the development of safety guidelines for HFCV in tunnels.

2. Problem Statement

Figure 1 shows a 3D tunnel dimensioned 5 m × 5 m × 102 m considered in this study. A 0.5 m × 0.5 m × 5 m solid inert rectangular object is centred in the middle of the tunnel cross-section with the 0.25 m^2 burner surface on the end, facing downstream towards the tunnel exit, positioned at 40 m, similar to Gu et al. [6].

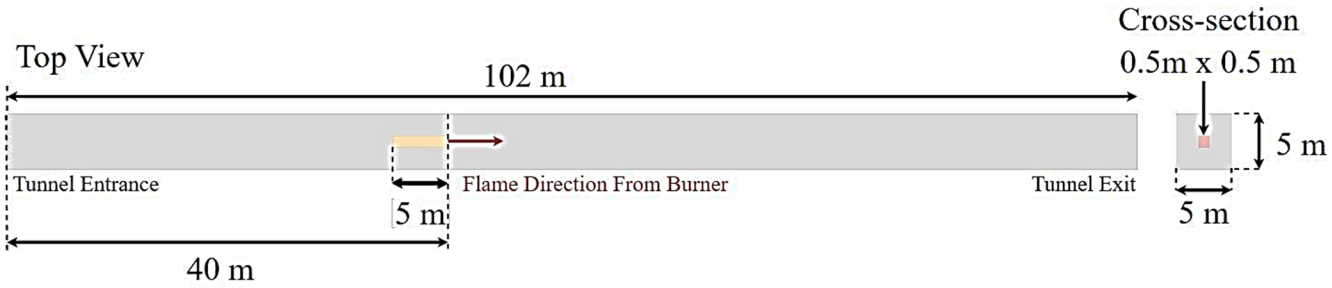

Figure 1. Schematic view of the dimensional layout.

The effects of tunnel slope, fire position, and ventilation (both longitudinal and transverse) are deemed critical parameters to develop a comprehensive understanding of the dangers presented by an HFCV, gaseous hydrogen jet fire, in an accidental scenario. A summary of all parameters for different scenarios is given in Table 1. For simplicity in the discussion, reference codes are assigned to each simulation with letters indicating testing parameters followed by the respective magnitude as follows: PO (Position), L (Longitudinal ventilation), T (Transverse ventilation), and S (Slope).

The 40 MW power is assumed to capture a severe scenario of a jet fire, which is consistent with the magnitude of HFCV fires in which an HRR is produced somewhere around 4 MW to 43 MW, depending on the mass flow rate, storage capacity and environmental conditions [5,23,24]. The mass flow rate registered for the 40 MW hydrogen fires is 0.282 kg/s [15]. Burner positioning of 25 m and 15 m from the tunnel entrance are deemed suitable in comparison to the 40 m as altered air supply/cooling by position would be expected to affect the results. Ventilation values were chosen to provide enough variation for confirmation of the existence of a critical velocity and the effects of variation in longitudinal and transverse ventilation on the severity of the scenario. All transverse ventilation studies are in conjunction with longitudinal ventilation to represent realistic scenarios. Referenced literature review values of slope in correlation to tunnel slope regulations are used to predict the suitable chosen values [23,25].

The simulations are run for a total time of 45 s, and results were recorded accordingly. It was found the results reach a quasi steady-state at about 15–20 s, and it remains in that state for the rest of the simulation (t = 45 s), which is consistent with the studies conducted previously [13–15]. Hence, the results over the quasi steady-state period are employed for the risk analysis where the expected temperature field of the entire tunnel was achieved, imposing the possible highest risk in the domain.

Table 1. A summary of parameters.

Case No.	Power (MW)	Burner Position (Distance from the Entrance) (m)	VentilationLongitudinal Velocity (V_L) (m/s)	VentilationTransverse Velocity (V_T) (m/s)	Slope (%)
1	6	40	2.5	0	0
2	40	40	2.5	0	0
3	40	15	2.5	0	0
4	40	25	2.5	0	0
5	40	40	0	0	0
6	40	40	5	0	0
7	40	40	0	0	3
8	40	40	2.5	0	3
9	40	40	2.5	0	5
10	40	40	2.5	1	0
11	40	40	2.5	2.5	0
12	40	40	2.5	1	3
13	40	40	2.5	1	5

3. Methodology

A numerical approach to risk assessment of HFCV jet-fire scenarios is developed to understand the effects of different tunnel characteristic parameters on both probabilities of burn injury and heat mitigation. As shown in Figure 2, the present methodology can be divided into two parts: (i) The CFD simulations are adopted to develop results assisting to analyse the dependency of jet-fire scenario severity on the chosen tunnel parameters. CFD simulations also produce detailed data that enhance the understanding of hydrogen jet fire. A large eddy simulation (LES) approach is adopted, and the simulations are conducted using Fire Dynamics Simulator (FDS) for different scenarios (see Table 1) to generate temperature fields and radiative intensity within personnel occupied areas along the tunnel. (ii) The collected CFD data is then processed and used within probabilistic and risk assessments on HFCV jet-fire incident severity in the tunnel. Further details are provided in the following sections.

3.1. Computational Approach

As shown in Figure 2, the primary step is set to conduct a comprehensive parametric study using CFD simulations. FDS, an open-source CFD software, is used that adopts LES to solve continuity, momentum, energy, and species mass balance [26,27]. In the following, the CFD methodology is further discussed.

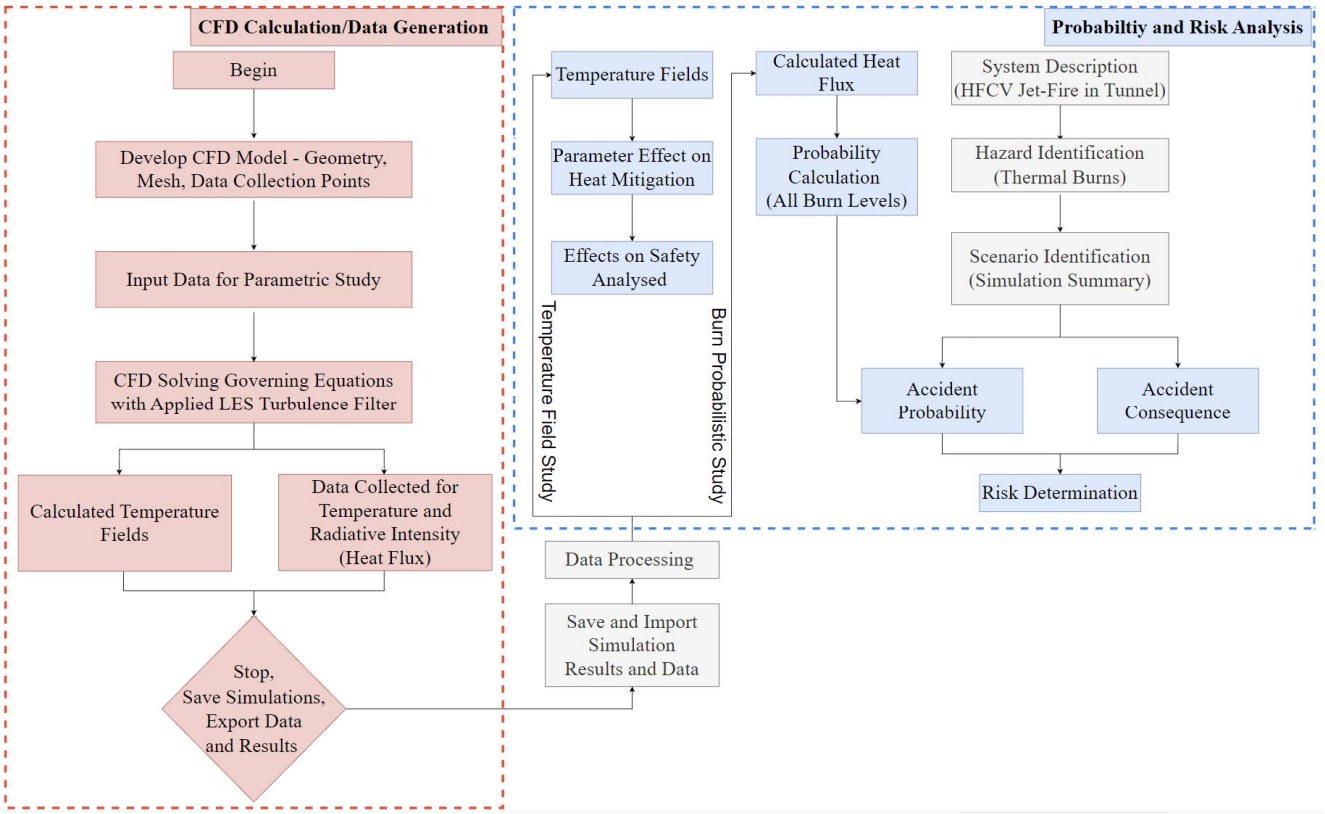

Figure 2. Methodology flowchart.

3.1.1. Governing Equations

The Favre filter balance equations of mass, momentum, energy, and species are [28].

$$\frac{\partial \overline{\rho}}{\partial t} + \frac{\partial}{\partial x_i}(\overline{\rho}\widetilde{u_i}) = 0 \tag{1}$$

$$\frac{\partial \overline{\rho}\widetilde{u_i}}{\partial t} + \frac{\partial}{\partial x_i}(\overline{\rho}\widetilde{u_i}\widetilde{u_j}) + \frac{\partial \overline{\rho}}{\partial x_j} = \frac{\partial}{\partial x_i}\left[\overline{\tau}_{ij} - \overline{\rho}\left(\widetilde{u_i u_j} - \widetilde{u_i}\widetilde{u_j}\right)\right] \tag{2}$$

$$\begin{aligned} &\frac{\partial \overline{\rho}\widetilde{h_s}}{\partial t} + \frac{\partial}{\partial x_i}\left(\overline{\rho}\widetilde{u_i}\widetilde{h_s}\right) = \frac{\partial \overline{p}}{\partial t} + \overline{u_i\left(\frac{\partial p}{dx_i}\right)} + \frac{\partial}{\partial x_i}\left[\overline{\lambda\frac{\partial T}{dx_i}} - \overline{\rho}\left(\widetilde{u_i h_s} - \widetilde{u_i}\widetilde{h_s}\right)\right] \\ &+\overline{\tau_{ij}\frac{\partial u_i}{\partial x_j}} - \frac{\partial}{\partial x_i}\left(\overline{\rho\sum_{k=1}^{N} V_{k,i}Y_k h_{s,k}}\right) + \overline{\dot{\omega}_T} \qquad where:\ k = 1, \mathrm{N} \end{aligned} \tag{3}$$

$$\frac{\partial\left(\overline{\rho}\widetilde{Y_k}\right)}{\partial t} + \frac{\partial}{\partial x_i}\left(\overline{\rho}\widetilde{u_i}\widetilde{Y_k}\right) = \frac{\partial}{\partial x_i}\left[\overline{V_{k,i}Y_k} - \overline{\rho}\left(\widetilde{u_i Y_k} - \widetilde{u_i}\widetilde{Y_k}\right)\right] + \overline{\dot{\omega}_k} \tag{4}$$

where the tilde (~) represents an applied filter and ($\overline{\ }$) denotes being averaged. ρ is the fluid density, t is time, u is the flow velocity, p is pressure, τ_{ij} is the viscous stress tensor, h_s is the sensible enthalpy of the mixture, λ is thermal diffusivity, Y_k is the species mass fraction, $\overline{\dot{\omega}_k}$ is the reaction rate for reacting species k, T is temperature, and V_k is the diffusion velocity of the species k. To close sub-grid scale (SGS) momentum terms ($\widetilde{u_i u_j}$), the gradient diffusion assumption is used, which employs the Smagorinsky turbulence model. Turbulent diffusivity is obtained using the Prandtl number (representing the thermal diffusivity) and the Schmidt number (representing the mass diffusivity). The Eddy Dissipation Concept (EDC) combustion is implemented for turbulence-chemistry interactions with a one-step reaction fast chemistry model [15,20,28].

3.1.2. Numerical Setup

The model is developed as a large-scale tunnel fire, with the tunnel entrance set as a supply with the air of uniform velocity and exit considered as an open surface allowing escape [6,13]. Surrounding mesh walls of the tunnel and combustion object (except the burner area) are considered inert. A Smagorinsky Constant is assumed 0.2, and $0.8 \leq \text{CFL} \leq 1$ is utilised in the consideration of LES. Initial temperature, pressure, and relative humidity are set to 20 °C, standard atmospheric pressure (101,325 Pa), and 40%, respectively. The mass fractions of O_2 and CO_2 are assumed 0.232378 and 5.95×10^{-4}, respectively [15].

Data collection points for temperature and thermal radiation (integrated intensity) are incrementally lined along the centre of the ceiling and at 1.5 m from the floor. The value is chosen from the assumption of the average height of a male and female being 1.77 m, and 1.63 m is considered for the heat flux, which would be experienced by the majority of personnel within the tunnel directly.

3.1.3. Mesh Verification and Model Validation

A structured mesh is adopted for the numerical analysis. Mesh refinement is carried out around important areas, such as the nozzle/burner and ceiling. A coarser mesh is generated around the point of less interest to reduce the computational demand. Around the burner and immediate ceiling, a cell size of 0.397 m is utilised, progressing to 0.5 m along the closer regions to the burner, and progressing to 0.630 m in regions of lesser interest. All corresponding meshes are ensured to be in whole-number ratios to minimise error within the calculation.

A mesh independence study is conducted on the averaged integrated intensity for three different mesh configurations (837,000, 1,413,600, and 1,793,600 cells) as HRR = 40 MW to ensure the results are not sensitive to the mesh size. Figure 3 shows that the mesh size initially affects the numerical results of the averaged radiative flux at 1.5 m over 45 s. However, further refinement over 1,413,600 cells shows a negligible impact on the results. Therefore, it is determined that 1,413,600 cell mesh is suitable to provide accurate results and save computing costs.

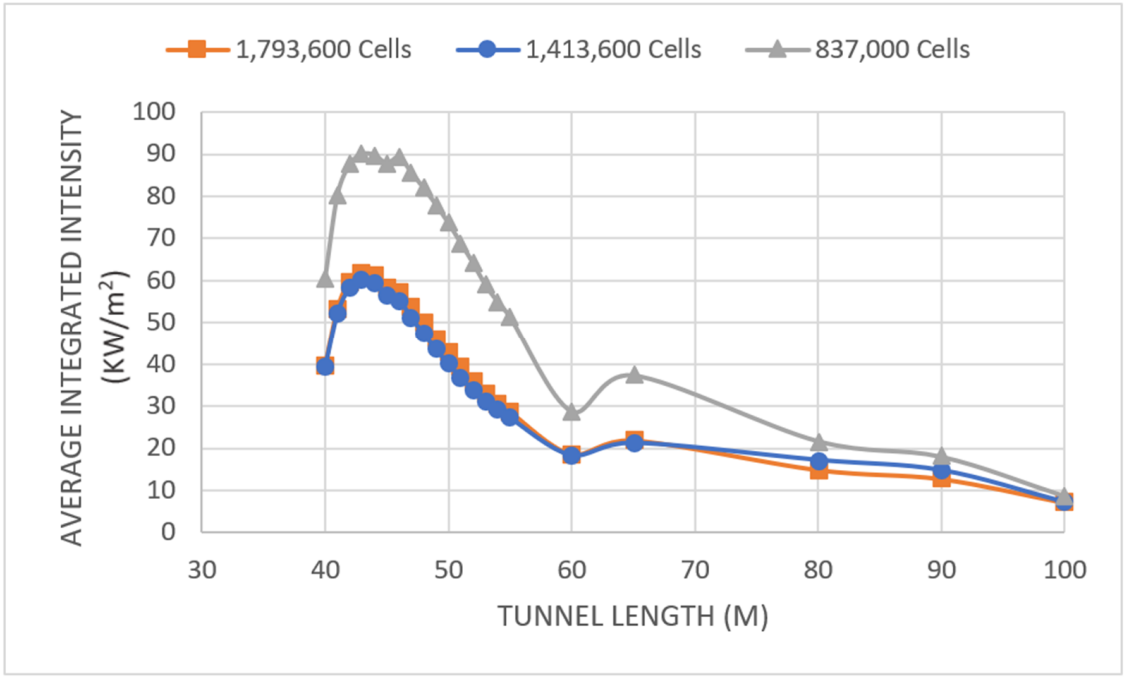

Figure 3. Radiative flux (integrated intensity) along the tunnel.

The validation of the present methodology with previous studies is carried out by comparing numerical results for the averaged mole fraction with the numerical results presented in [6]. The model is set up as shown in Figure 1, with a 2.5 m/s longitudinal ventilation supplied from the entrance of the tunnel while the heat release rates (HRRs) are 6 and 30 MW. Sensor points collect the volume fraction incrementally along the centre of the ceiling of the tunnel distance. The hydrogen concentration is shown in Figure 4 for both validation cases. Reasonable compatibility is achieved for the case of HRR of 6 MW. The peak value is well captured while its location is slightly behind the previously modelled data, which could be due to the variation in cell density and number between models and/or the burner geometry. Similarly, the present model predicts the average mole fraction against the tunnel length with an acceptable agreement for the HRR of 30 MW. However, the decay rate is predicted slightly faster than the previous study [6] for distances over 55 m.

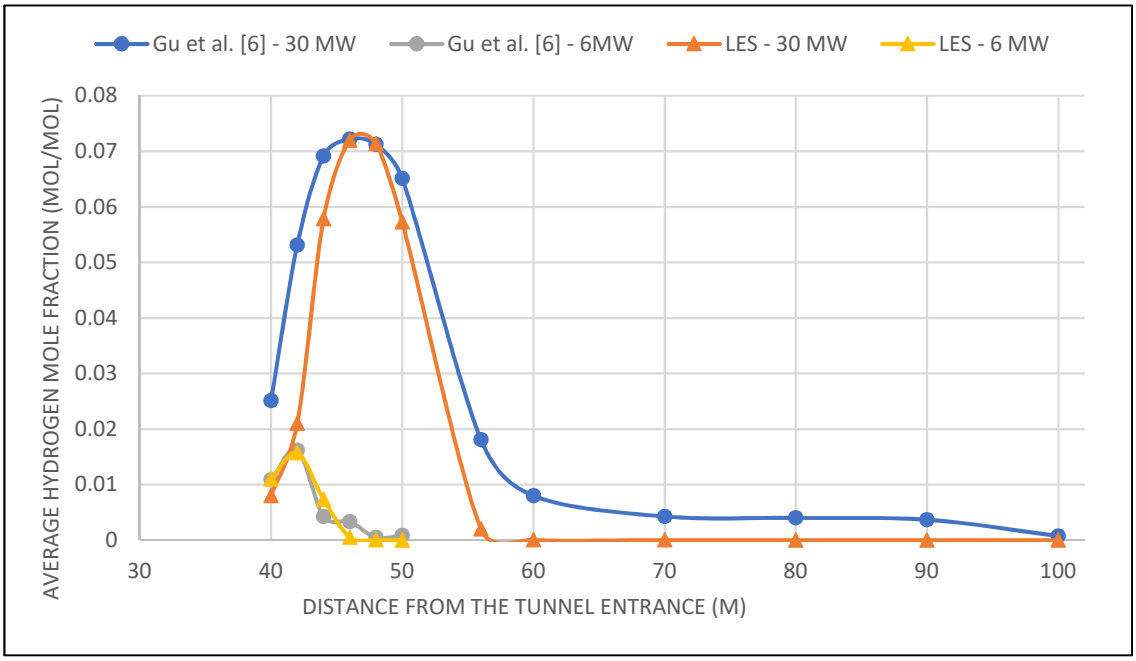

Figure 4. Hydrogen mole fraction along the tunnel—validation case.

3.2. Probability Assessment Method

The risk assessment process flow incorporated within Figure 2 is chosen to facilitate the comprehensive capture of risk characteristics [7,29]. The assessment of the radiative intensity on human life closely follows M.J. Assael Fires, Explosions and Toxic Gas dispersion, effects calculations, and risk analysis [30]. This method effectively captures the consequence and risk to personnel at varying distances from the incident through integrated intensity measured by the LES [19].

Flux results are then integrated into the following probabilistic calculations to determine the severity of the outcome of the hydrogen jet fire scenario. The chosen value to be used as the heat flux q' of Equation (8) is determined by the maximum flux at 1.5 m height (personnel location range) over the period where a quasi-steady state is achieved. This is to ensure that the encapsulation of the severity of the scenario to highlighting the worst case of thermal radiation presented by the CFD analysis.

Probabilities of impacts from the incident (P_i), explained in Table 2, can be broken down into first-degree burn, second-degree burn, and death, calculated using Equation (5) [30].

$$P_i = F_k \frac{1}{2} \left[1 + eff\left(\frac{Pr - 5}{\sqrt{2}} \right) \right] \quad (5)$$

where Pr is the Probit function applied to the probability, F_k is the correction factor for clothing, and *eff* is the error function determined by Assael et al. [30], expressed as follows:

$$\Pr = c_1 + c_2 ln(D) \tag{6}$$

$$\begin{gathered} eff(-z) = -eff(z).\ For\ z > 0\ and\ error < 5 \times 10^{-4} \\ eff(z) = 1 - \left(1 + 0.278393z + 0.230389z^2 + 0.000972z^3 + 0.078108z^4\right)^{-4} \end{gathered} \tag{7}$$

where c_1 and c_2 are Probit Function coefficients selected based on Table 3, D is the thermal radiation dose ($W^{\frac{4}{3}}\ s \times m^{-\frac{8}{3}}$). Equations (8) and (9) describe the calculation of thermal radiative dose D required to calculate Equation (9).

$$D = t_{eff}\left(q'\right)^{\frac{4}{3}} \tag{8}$$

$$t_{eff} = t_r + \frac{x_o - r}{u_e} \tag{9}$$

where t_{eff} is the exposure time (s) which is dependent on the distance of the person from the incident flame. q' is the heat flux (W/m^2), t_r is a person reaction time (usually = 5 s [30]), x_o is the distance between the lame surface and position where intensity flux is lower than 1 kW/m^2, r is the distance from flame to person (m), and u_e is the escape velocity (usually 4 m/s [30]). Heat flux ($q^{'}$) is determined through LES simulations with reference to Table 4 on the severity of the incident.

Table 2. Thermal radiation consequence description [19].

Effect Type	Damage
First Degree Burn	Affects the outer layer of the skin (epidermis). Dry, red, painful, minimal blistered skin. Superficial wounds with long-term damage are rare. An example of this is mild sunburn.
Second Degree Burn	Effects deeper layer of skin (dermis—0.07–0.12 mm depth) as well as the epidermis. The wound is painful, red, blistered skin, and may be swollen.
Death	Fatality

Table 3. Probit function coefficients [30].

Effect Type	C2	C2
First Degree Burn	−39.83	3.0186
Second Degree Burn	−43.14	3.0186
Death	−36.38	2.56

Table 4. Heat flux intensity effects on humans [19].

Heat Flux (kW/m^2)	Effect on Humans
32.5	100% Lethality in 1 min 1% Lethality in 10 s.
25	100% Lethality in 1 min Serious injuries in 10 s.
12.5	1% Lethality in 1 min First-degree burns in 10 s.
4	No Lethality. A second-degree burn is probable. Pain after 20 s of exposure.
1.6	The acceptable limit for prolonged exposure.

A risk index is calculated through Equation (10) and its assigned risk score (S_i) is obtained from Table 5 [19]. Then, the probability of each scenario occurring can be obtained as

$$Risk_i = S_i \times P_i \tag{10}$$

Table 5. Risk score chart [19].

Effect Type	First Degree Burn	Second Degree Burn	Death
Risk Score	2	5	10

Further development and analysis of possible accidental scenarios and their variations can be performed using risk assessment tools such as event sequence diagrams (ESD). Figure 5a displays the probability of a hydrogen jet-fire incident within a tunnel accident and an effective continuation means for the holistic probability of events within such an accident. The foundational probabilities of hydrogen jet fire within a tunnel per million vehicle miles (MVM) are outlined by the red line.

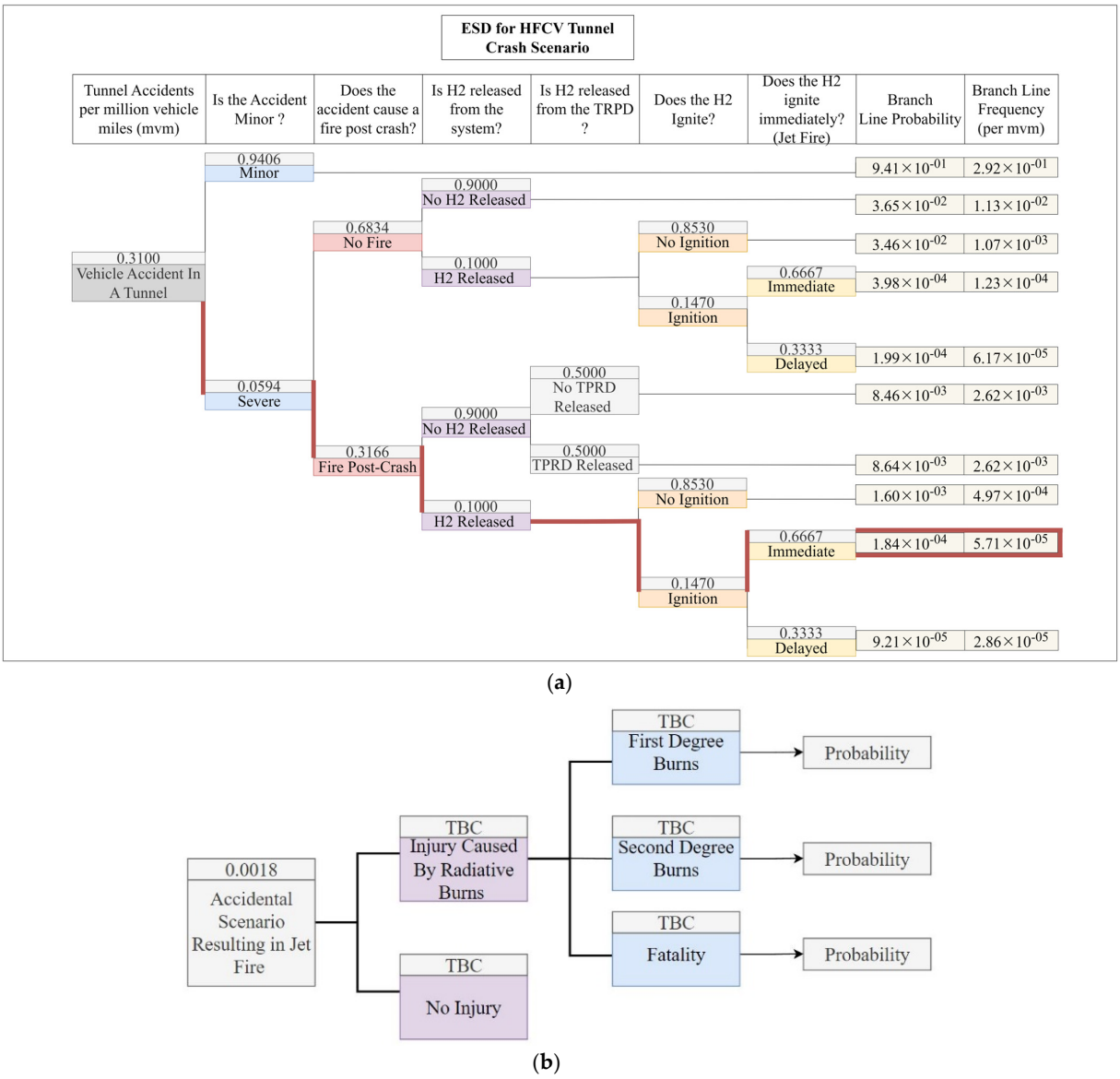

Figure 5. (**a**) ESD for HFCV Tunnel crash scenario [16] and (**b**) Thermal radiation burns probability ESD continuation. TBC—To Be Calculated.

It is demonstrated the probability of an external hydrogen jet fire scenario displayed through the trace of the red line, is 0.00018 which is obtained using the ignition probably of 14.7% determined by the Canadian Hydrogen Safety [16]. They used an estimation of the averaged probabilities of immediate and delayed ignition [16]. However, it should be noted that actual hydrogen release rates and ignition are incident-specific data and should be critiqued before direct use [19,31].

Using calculated values of hydrogen jet-fire likelihood within a tunnel per MVM, an extension can be captured through the use of Figure 5b and Equation (11). A holistic probability is then obtained using the probability of a hydrogen jet fire ($P_{Accident(mvm)}$) in a tunnel with the calculated probability of impact of thermal injury (P_i) [16]:

$$P_{Total} = P_{Accident(mvm)} \times P_i \tag{11}$$

4. Results and Discussion

First, a parametric study is comprehensively conducted to identify the impacts of significant parameters in the tunnel, analysed by computational results, including the tunnel temperature and velocity contours at 45 s. Then, the probabilistic study provides a direct indication of personnel safety within the accidental scenario in which an understanding of HFCV tunnel fire severity is gathered.

4.1. LES Results

The ability of the tunnel system under test to eject accumulated heat can be seen by the effects of back-layering within the scenario and fluctuation of heat height along the tunnel [15]. Back-layering provides a good indication of entrapped heat within the system, and therefore less back-layering shows evidence of an effective means of ejecting heat. Less fluctuation of heat height is essential as it ensures less heat enters the height/domain where personnel reside. Hence, the back-layering effects are discussed in detail using the LES results to shed some light on the phenomena as the influencing parameters vary.

4.1.1. Effects of Tunnel Slope

The evolutionary trend of the maximum temperature over the duration of 45 s is taken along the ceiling of the tunnel. As seen in Figure 6a, an increase in slope results in a decrease in the maximum ceiling temperature. Since the heated gas travels a further distance before the incident with the ceiling, a greater amount of cooling time and distance can be seen in agreement with similar studies of LPG [23]. With considerable differences of 100–200 °C per slope variation, it is a significant characteristic when reviewing tunnel fire safety as temperatures can reach well above damaging and danger thresholds for assets (structural and vehicular) and personnel. Li et al. [25] showed that the tunnel slope should not exceed 5% in the traffic when the design vehicle speed is over 50 km/h since the flame tilt angle varies with the tunnel slope affecting the maximum ceiling temperature and steady-state gas temperature [23]. Shibani et al. [15] found that an increase in the tunnel slope intensifies the fire severity in high-temperature zones.

The effect of the tunnel slope on back-layering is further discussed by the average temperatures. The back-layering causes heat entrapment and an increase in average temperatures within a specific ceiling location. An average of ceiling temperatures over 45 s effectively captures the accumulations of heat and back-layering and slope effectiveness at mitigating heat shown in Figure 6b. The average temperatures over the simulation time demonstrate an increase in temperature just behind the nozzle. This is understandable as the slope prevents back-layering from occurring and in turn an accumulation of higher heat just before the nozzle.

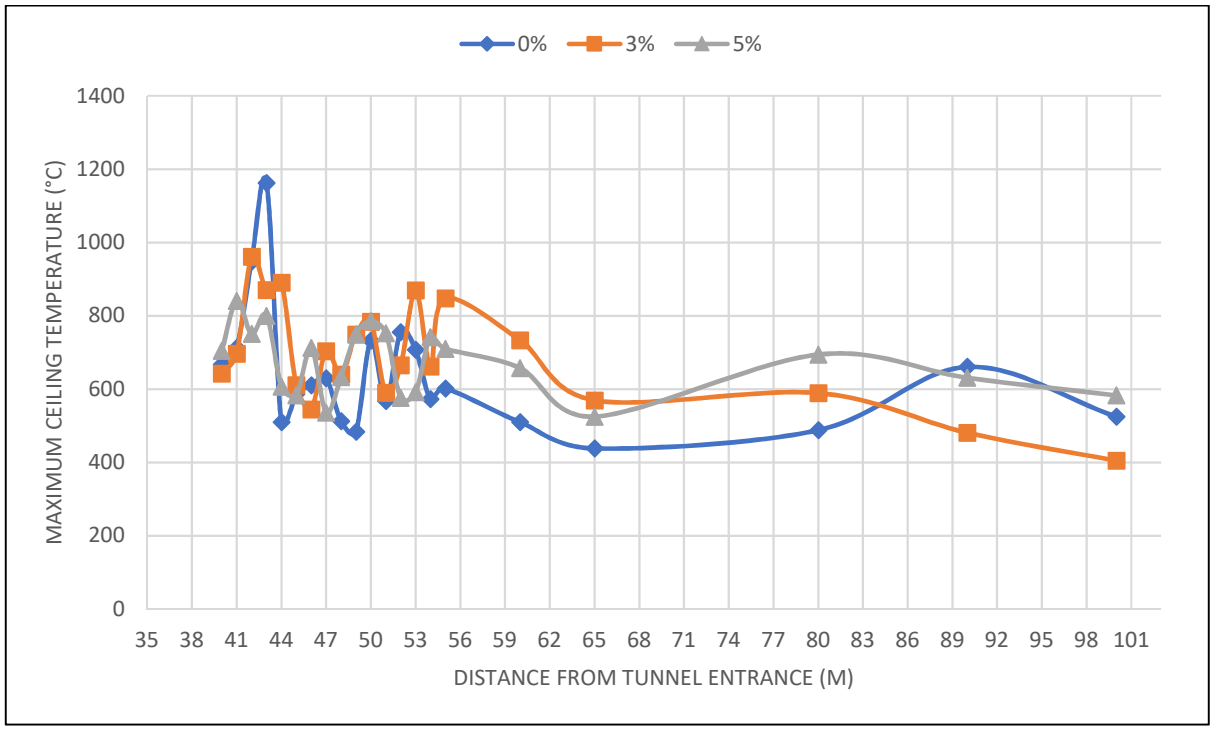

(**a**)

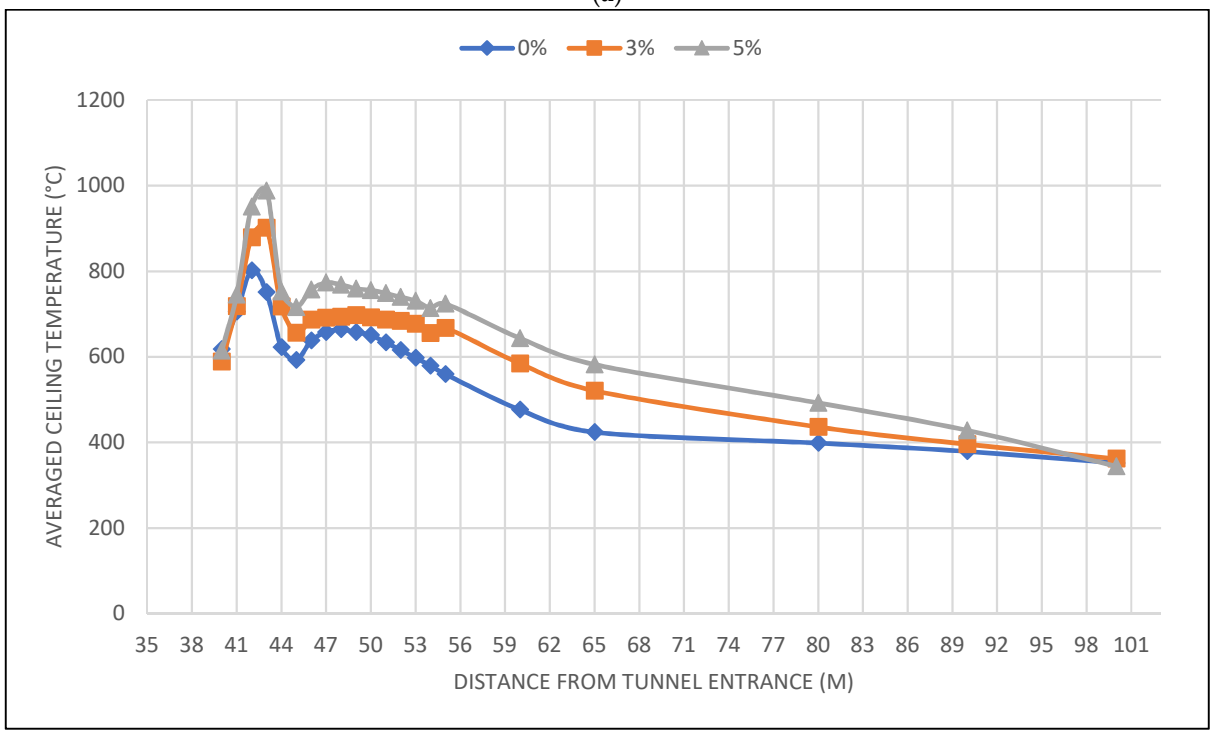

(**b**)

Figure 6. (**a**) Maximum ceiling temperatures and (**b**) Averaged ceiling temperatures along the tunnel at $V_L = 2.5$ m/s, $V_T = 0$ m/s—effect of tunnel slope (Cases 2, 8 and 9).

Figure 7 shows the temperature and velocity fields at 45 s in the tunnels. The tunnel ceiling is maintained at a lower temperature as the cooler gases are constantly replaced with the heated gases. Interestingly, higher temperatures can be seen downstream of the fire, which may attribute due to the higher velocity and less cooling time of heated gases caused by the slope. When the velocity of ventilation is low, it allows hot gas generated

by fire to move back upstream in the opposite of the ventilation direction, known as back-layering [32]. Back-layering demonstrates inefficiencies in the removal of heat from a tunnel and, in turn, may lead to a greater risk of property damage or personnel injury. The temperature fields show that higher temperatures can be seen downstream of the fire as the slope increases, which may attribute due to the higher velocity and less cooling time of heated gases caused by the slope. A closer look indicates that the tunnel slope has a direct effect on the temperature distribution and ejection of heat within a gaseous hydrogen tunnel jet fire scenario. Increasing the tunnel slope from 1 to 3% results in a reduction of 7.4 m in back-layering, while further increase reduces it to 8.2 m (marked by solid vertical lines in Figure 7). In addition, an increase in the tunnel slope mitigates the effect of the circulation of heated air/gas upstream of the flow.

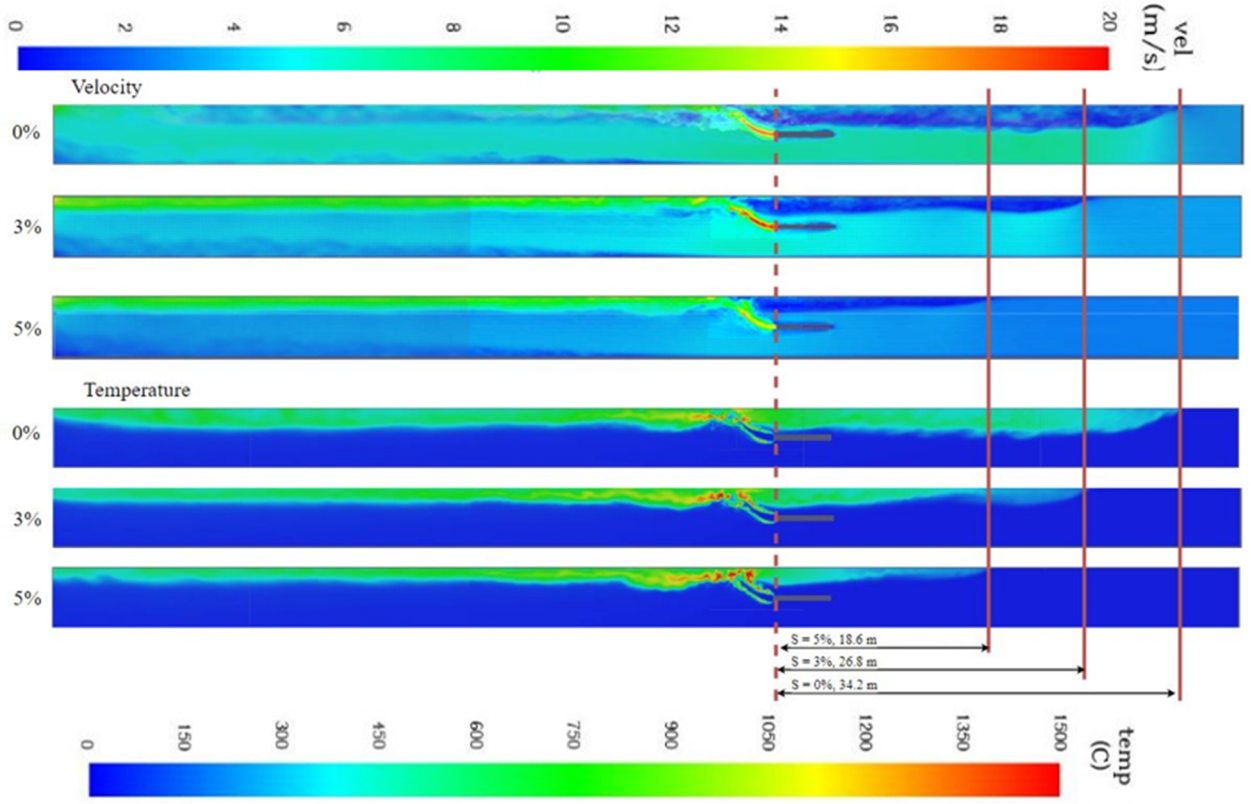

Figure 7. 2D temperature and velocity contour plots at 45 s–effect of tunnel slope (Cases 2,8, and 9).

4.1.2. Effects of Fire Source Location

The critical velocity is termed by the minimum longitudinal ventilation required to overcome back-layering and remove hot gases from the opposite of the ventilation direction [33]. Figure 8 presents the effects of the fire position from the entrance on the heated gas accumulation in a tunnel for three cases, 15 m, 25 m, and 40 m, in which an increase in back-layering occurs when the fire location is closer to the entrance. As can be seen in the velocity and temperature contours, the longitudinal ventilation at the inlet is higher than the critical flow of the back-layering gases resulting in a thicker accumulation of heat. Additional testing of this parameter is suggested as domain sensitivity may also have a role to play with the interesting result of back-layering for fire positions 15 m and 25 m ending at approximately the same point.

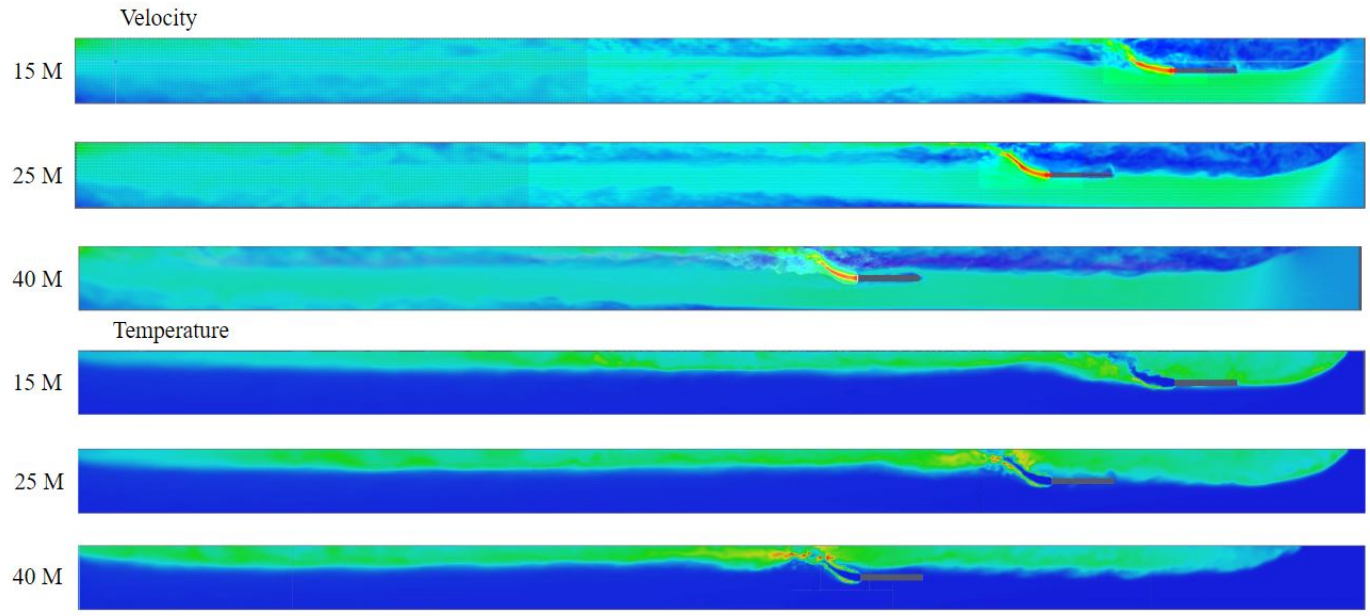

Figure 8. 2D temperature and velocity contour plots at 45 s–effect of the fire source location (Cases 2, 3, and 4). The colour code is the same as in Figure 6.

4.1.3. Effects of Longitudinal and Transverse Ventilation

In addition to the ventilation essential for normal operation in tunnels, emergency ventilation is critical to reducing the risk of heat and smoke in the case of a fire [14,22]. We first study the impact of longitudinal ventilation velocity. While the longitudinal ventilation velocity varies, the transverse ventilation velocity is zero (Cases 2, 5 and 6 in Table 1). Figure 9 shows that an increase in longitudinal ventilation results in a larger flow of cool air into the system, displacing heated gas/air. A longitudinal airflow of 5 m/s is well above the critical velocity and, as a result, minimises the back-layering effect to nil. Notably, a comparison of no ventilation to 2.5 m/s longitudinal ventilation indicates a thicker back-layer which may result in more danger upstream of the fire. With an overall fluctuation downstream being increased with the larger longitudinal flows, results suggest longitudinal ventilation alone may increase possible danger downstream of the flow which is further analysed in the probabilistic study.

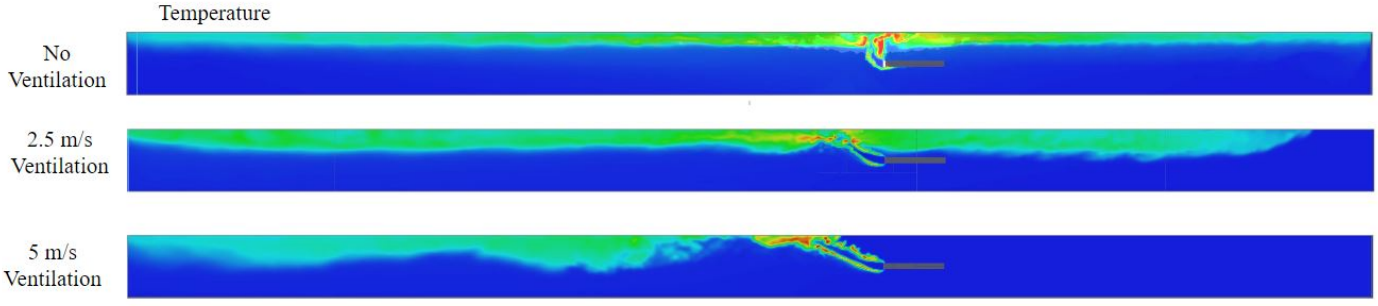

Figure 9. 2D temperature and velocity contour plots at 45 s—effect of the longitudinal ventilation velocity (Cases 2, 5, and 6). The colour code is the same as in Figure 7.

Further analysis is conducted on the effect of tunnel transverse ventilation (Cases 2, 10, and 11 in Table 1). Figure 10 shows that the effect of transverse ventilation has a significant impact on the back-layering of the heated gas/air with all cases longitudinal ventilation at 2.5 m/s. In addition, combined longitudinal and transverse ventilation increases the stability of heat flow in both upstream and downstream directions within the tunnel. A possible reason for this result is that the ventilation provides enough upwards pressure

to minimise the downward fluctuation of the turbulent heat flows. However, it is evident that the resulting back-layering due to rising transverse ventilation from zero to 2.5 m/s is much thicker and, as a result, resides lower, encapsulating a higher heat concentration with the addition of transverse ventilation, which may contribute to a higher risk behind the burner.

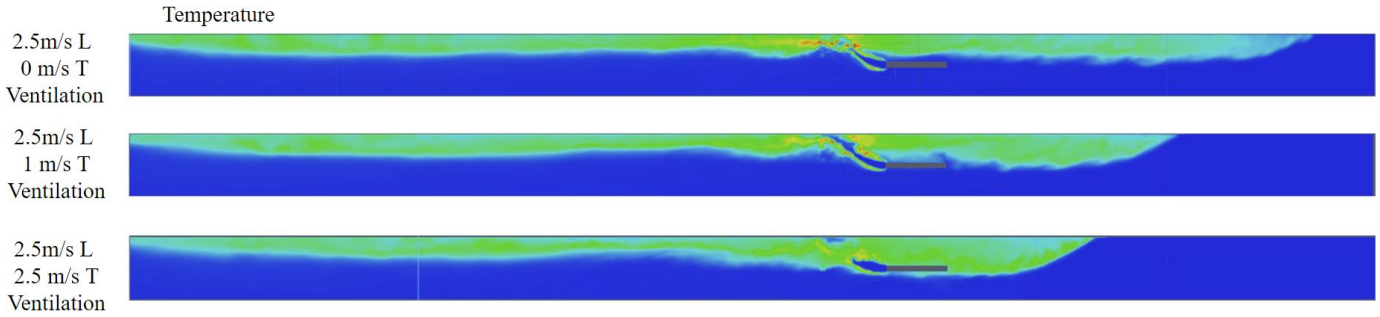

Figure 10. 2D temperature and velocity contour plots at 45 s—effect of the transverse ventilation velocity (Cases 2, 10 and 11). The colour code is the same as in Figure 7.

We also analysed the impact of combining the transverse ventilation and the tunnel slope at the constant longitudinal ventilation of 2.5 m/s on the back-layering. In Figure 11, the resultant temperature contours suggest an effective combination of tunnel characteristic variables to mitigate the back-layering effect and heat of a gaseous hydrogen fire within the tunnel. It can be also noted that the heat profile is maintained at a closer range to the roof which results in a lower risk of burns further down the tunnel. This is an important consideration as it can minimise the exposure to radiation and thermal energy for personnel escaping the incident. Therefore, a combination of longitudinal and transverse ventilation with an increased slope poses a very effective way to mitigate the heat produced by the fire in the tunnel at a fast but also stable rate, resulting in possibly the safest solution when dealing with HFCV tunnel fire scenarios.

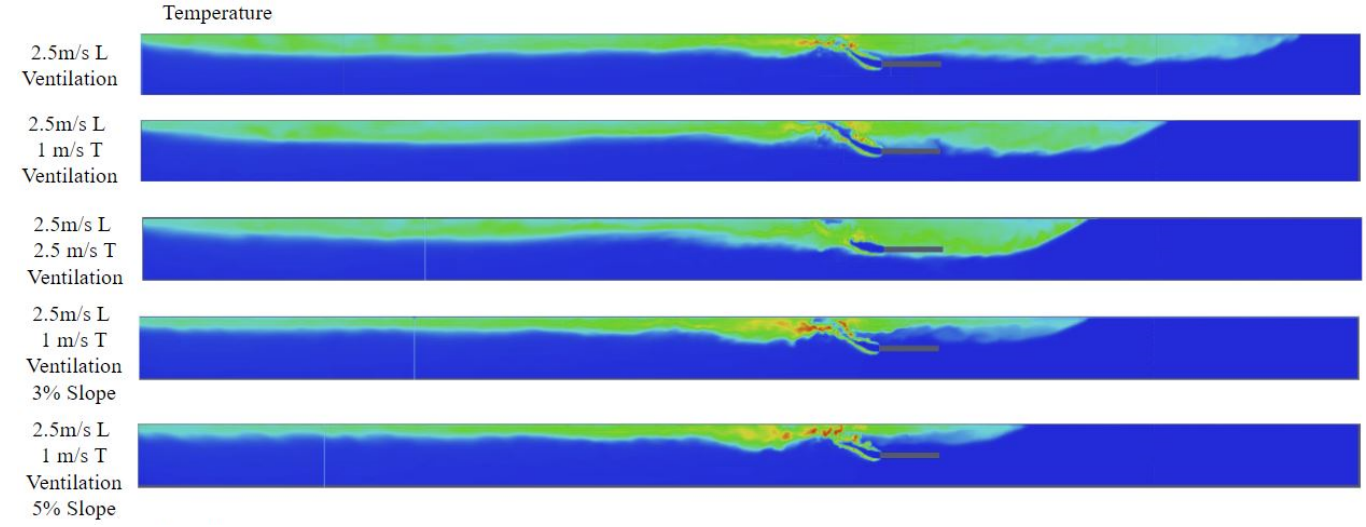

Figure 11. 2D temperature and velocity contour plots at 45 s—the combined effect of the influencing parameters (Cases 2, 10, 11, 12, and 13). The colour code is the same as in Figure 7.

It can be seen that this combination is effective at minimising the thickness of the back-layering whilst also ensuring safe flows downstream. Comparing flows with the presented back-layering determines with a slope of greater than 3% a back-layering reduction can be achieved in a safer manner than that of flows with higher transverse ventilation alone.

Further, it supports that slope is one of the primary design parameters essential when tunnel design and ventilation techniques are placed under consideration.

4.2. Burn Probability Analysis

The probabilistic calculation is then performed. The stability of these Probit functions requires to be analysed with a discovery of a distance from the burner surface of 50–60 m testing being a limit through gathered results which may be attributed to the open outlet boundary causing such instabilities combined with the equations limits. Using an average of trends of the simulation data, the required input values are determined for each measurement, and a formulation of incidental probabilities of 1st, 2nd, and 3rd-degree burns are then developed.

Following probability calculation, it is found that the 40 MW fire chosen presented a very high risk with a probability of 1st-degree burn being at 100% over the duration of tunnel distance. In turn, for simplicity of the result digestibility, the probabilities of second-degree and third-degree scenarios are represented as P2 and P3. It is worth noting that these are the probabilities of injury within the event and not the combined total probabilities considered later. These probabilities are considered as they provide a good representation of the effects of the tunnel and environment variables on the severity of the outcome of an HFCV tunnel fire scenario.

As shown in Figure 12, the slope has a significant effect on the probability of a severe outcome which is in agreement with the temperature contours shown in Figure 7. It is concluded that the slope significantly mitigates the probabilistic injury risk through heated gas cooling travelling greater distances from the incident. It can also reduce the overall radiation experience by personnel from the heated gasses travelling along the roof. Moreover, these heated gases move with a higher velocity along the ceiling being less impeded resulting in less ambient heating and promoting more airflow (of cooler air). These results are in agreement with expectations and therefore provide conclusive evidence that slope affects the tunnel safety of an accidental HFCV jet fire scenario. For the purpose of more meaningful graphical measurement and representation, all figures in this section are shown from 50 m as all recorded data points are relatively the same between zero and 55 m.

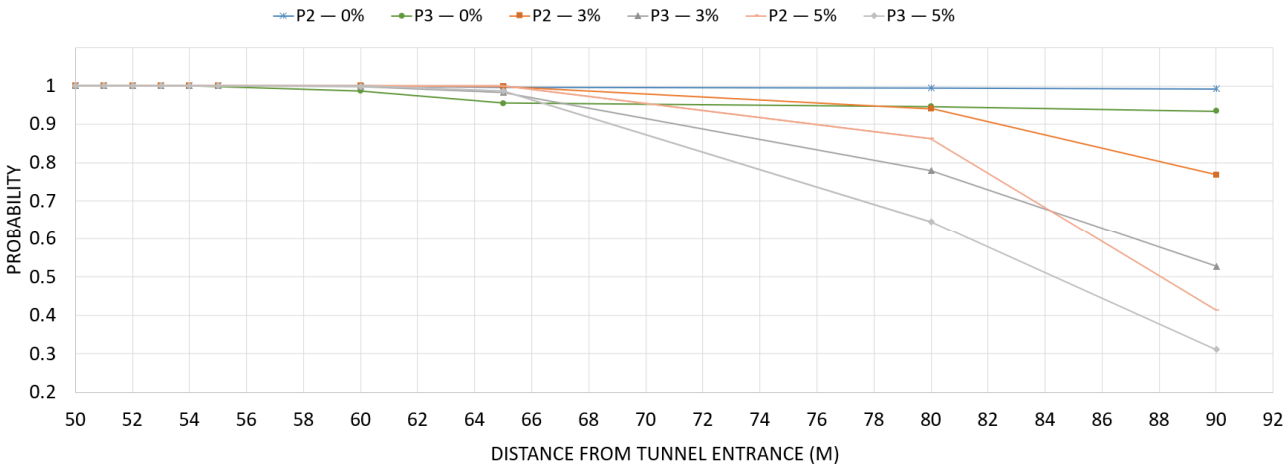

Figure 12. Slope comparison for probabilistic injury at $V_L = 2.5$ m/s, $V_T = 0$ m/s. P2 and P3 refer to the probability of second and third burn injuries, respectively.

Figure 13 compares three fire positions of 15, 25, and 40 m with the probabilities of second-degree and third-degree scenarios. Close distances to the entrance (airflow inlet) may promote safer conditions as shown by comparing the probability of the second and third burn for Case 3 (P2—15m and P3—15m) to their relative probabilities at different burner positions. It can be seen that a very close distance to the tunnel entrance reduces the

probability of the third burn degree by the comparison of 25 m and 40 m cases (P3—25 m and P3—40 m), in which the probability of injury is relatively unchanged understandably as the cooling effects on inlet flows are reduced and affected by back-layering.

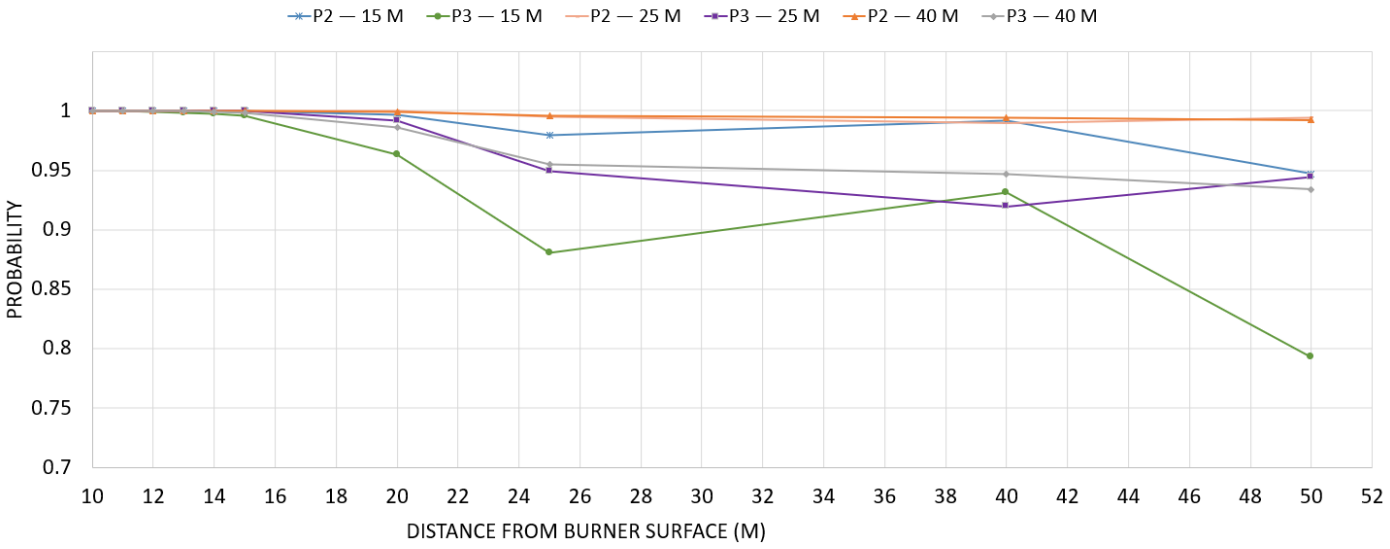

Figure 13. Fire position comparison for probabilistic injury at $V_L = 2.5$ m/s, $V_T = 0$ m/s. P2 and P3 refer to the probability of second and third burn injuries, respectively.

The LES results showed that longitudinal ventilation less than the critical velocity has negative effects on the safety scenario due to the back-layering and the accumulation of heat within the system [13,32]. Despite this, Figure 14a shows that high flow velocities may result in increasing the risk of burn injury downstream, by contributing to unsteady flow and causing heat to enter lower parts of the domain where personnel reside. High levels of longitudinal ventilation also promote greater mixing, assisting with combustion and as a result increasing danger. As shown in Figure 14b, transverse ventilation has a critical velocity that needs to be considered in relation to longitudinal ventilation values to quite understand fire safety in combined longitudinal and transverse ventilated tunnel systems. Additionally, fluctuations downstream at 80 m suggest that transverse ventilation can affect stable heat emission from the tunnel.

Further analysis is conducted for the combined effects as the LES results confirmed the dependency of tunnel parameters on the probability of burns. At the slope of 0 and 3%, the effect of combined ventilation is minimal with the maximum differences in the probability of approximately 1% when compared to the slope alone as seen in Figure 14b (T1) and Figure 15a. However, Figure 15b shows that the slope of 5% with combined ventilation may have a negative impact increasing dangers by up to approximately 15%. For all cases, the longitudinal ventilation is set to 2.5 m/s.

Combining the effects of the slope with both ventilation techniques of longitudinal and transverse ventilation shows promising in terms of the removal of heat. However, an effective solution to tunnel fire safety and removing heat in a safe manner must be ensured. Further research is recommended as results present a strong suggestion that critical combinations of these variables in magnitude and direction may present a further enhancement of tunnel fire safety.

In summary, understandably the total probability represents the same graphical trends presented in the above probabilistic figures. With the application of Equations (10) and (11), we found that a relative risk score of 10 in the first 25 m is presented for this extreme case with the calculated probabilities of third-degree burns being in the high 90 s to 100 percentiles. Applying Sandia's derived values for burns resulting from fire per mvm, we are presented with a common case of 0.00018 due to the calculated P_i. It is suggested

that further studies at lower HRR can be conducted using this method to continue the development of the HFCV QRA database.

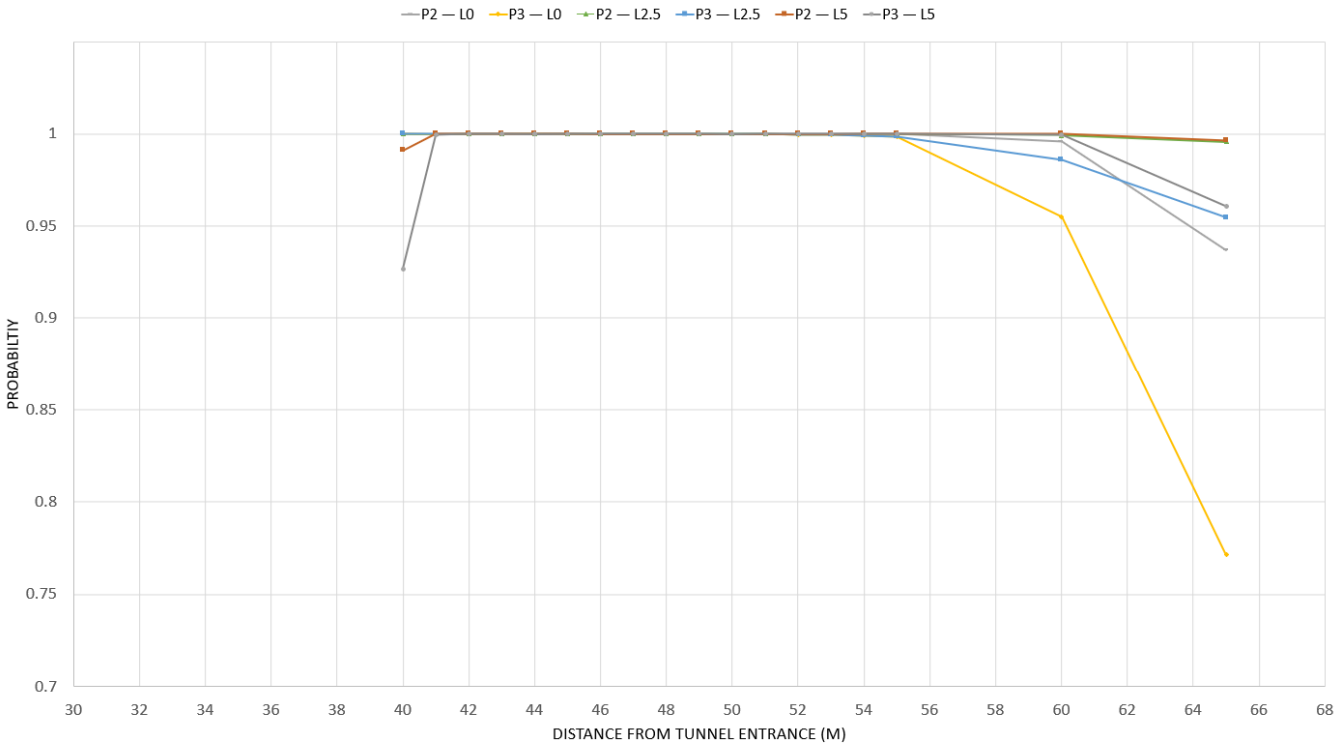

(**a**)

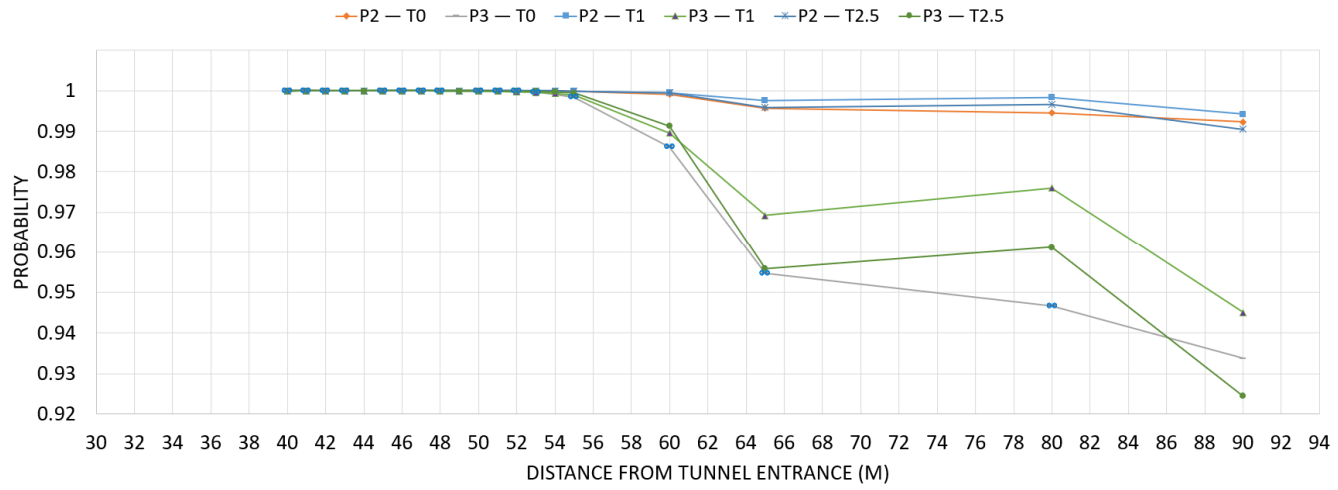

(**b**)

Figure 14. (**a**) Longitudinal ventilation comparison with $V_T = 0$ m/s. (**b**)—Transverse ventilation comparison with $V_L = 2.5$ m/s for probabilistic injury. P2 and P3 refer to the probability of second and third burn injuries, respectively.

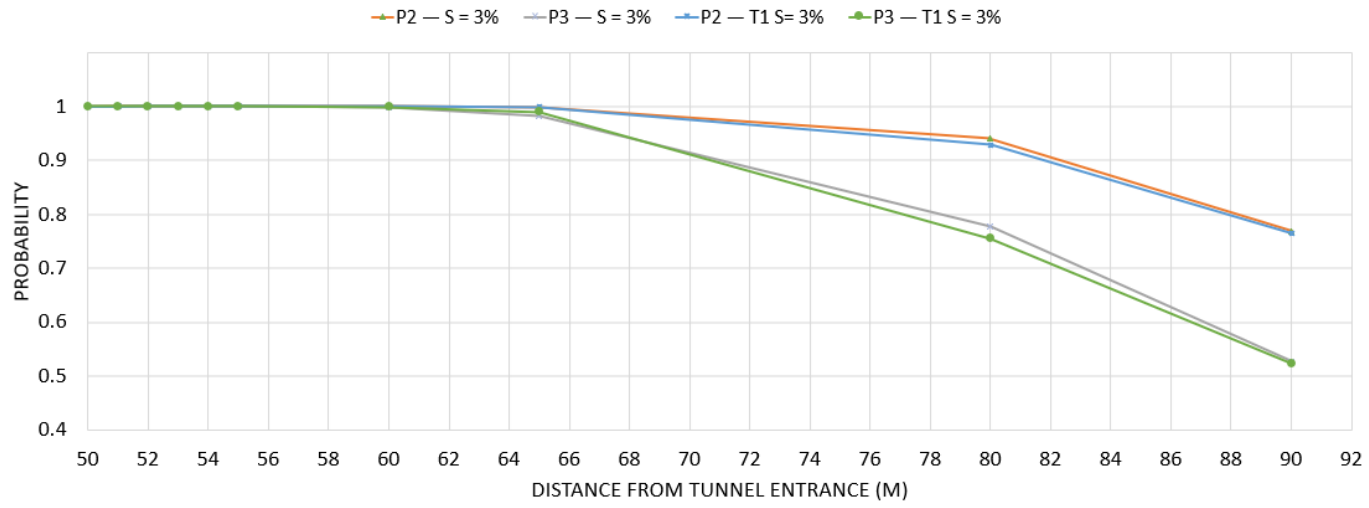

(**a**)

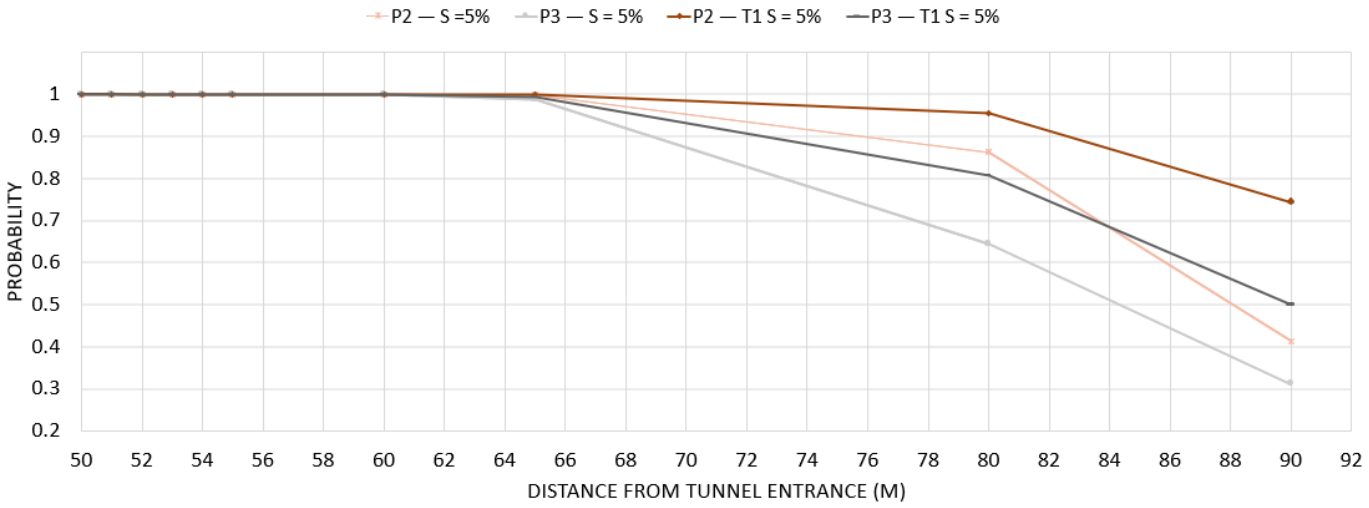

(**b**)

Figure 15. (**a**) 3% slope with $V_L = 2.5$ m/s compared to 3% slope with combined ventilations $V_L = 2.5$ m/s and $V_T = 1$ m/s. (**b**) 5% slope with $V_L = 2.5$ m/s compared to 5% slope with combined ventilations $V_L = 2.5$ m/s and $V_T = 1$ m/s. P2 and P3 refer to the probability of second and third burn injuries, respectively.

5. Conclusions

A new computational framework based on the large eddy simulation (LES) and probabilistic analysis was developed to analyse the risk of hydrogen fire accidents in semi-confined spaces. A parametric study was first conducted to analyse the impact of tunnel slope, fire position, and longitudinal and transverse ventilation. Then, LES data was incorporated to conduct the probabilistic calculation to determine the associated thermal risk of a hydrogen jet fire in a tunnel and its dependency influencing parameters.

As the slope of the tunnel increased, the back-layering effect was reduced in the scenario of ventilation being directed "uphill" of the tunnel slope. The tunnel slope also reduces incident temperature with the ceiling, while important considerations of entrapped heat circulation were identified by an increase in slope. In addition, the variation of the fire position in the tunnel was found with no notable benefits to probabilistic safety downstream from the fire. Positioning closer to the entrance resulted in thicker back-layering which

may contribute to higher dangers upstream of the fire. In terms of ventilation, combined transverse and longitudinal ventilation considerably reduced the back-layering effect. However, probabilistic studies confirmed that it had minimal effect on dangers downstream with higher concentrations of heat. Combined transverse and longitudinal ventilation with tunnel slope described promising results of removing heat in a relatively stable manner and reducing the dangers of the scenario downstream.

It was shown that, at such a large power output of 40 MW, a hydrogen jet fire presented significant risks. It was also determined that prior to the large-scale implementation of this technology, further review and research are required to build upon the QRA to minimise potential consequences related to this technology. This is essential to minimise the severity of accidental scenarios and enable safe practices for first responders with HFCVs in emergency scenarios.

Future works may include the analysis of scenarios where multiple HFCVs and flame obstructions are presented. It is also important to conduct comparative studies focusing on both conventional vehicles and HFCVs to further develop comprehensive datasets for accurate QRA, assisting with the development of emergency procedures. Understanding that this study has made the assumption of a continuous flow of fuel with no study on fuel consumption within the tank, it is also important to further an understanding of scenarios that consider a limited fuel supply with a varying mass flow rate due to pressure changes.

Author Contributions: Conceptualization, F.S. and R.A.; methodology, B.V., F.S. and J.M.; software, B.V.; validation, B.V.; formal analysis, B.V.; resources, F.S.; writing—original draft preparation, B.V.; writing—review and editing, J.M., F.S. and R.A.; supervision, F.S. and J.M. All authors have read and agreed to the published version of the manuscript.

Funding: This research received no external funding.

Institutional Review Board Statement: Not applicable.

Informed Consent Statement: Not applicable.

Data Availability Statement: Data will be available upon request.

Conflicts of Interest: The authors declare no conflict of interest.

References

1. HSE. Safety Excellence in Energy Series. In Proceedings of the Safe Net Zero 2021—Hydrogen, online, 2–4 March 2021.
2. Najjar, Y.S. Hydrogen safety: The road toward green technology. *Int. J. Hydrogen Energy* **2013**, *38*, 10716–10728. [CrossRef]
3. Li, Y.Z. Study of fire and explosion hazards of alternative fuel vehicles in tunnels. *Fire Saf. J.* **2019**, *110*, 102871. [CrossRef]
4. Tolias, I.; Giannissi, S.; Venetsanos, A.; Keenan, J.; Shentsov, V.; Makarov, D.; Coldrick, S.; Kotchourko, A.; Ren, K.; Jedicke, O.; et al. Best practice guidelines in numerical simulations and CFD benchmarking for hydrogen safety applications. *Int. J. Hydrogen Energy* **2019**, *44*, 9050–9062. [CrossRef]
5. Molkov, V. Fundamentals of Hydrogen Safety Engineering I. 2012. Available online: https://bookboon.com/ (accessed on 7 August 2021).
6. Gu, X.; Zhang, J.; Pan, Y.; Ni, Y.; Ma, C.; Zhou, W.; Wang, Y. Hazard analysis on tunnel hydrogen jet fire based on CFD simulation of temperature field and concentration field. *Saf. Sci.* **2020**, *122*, 104532. [CrossRef]
7. Crowl, D.A.; Jo, Y.-D. The hazards and risks of hydrogen. *J. Loss Prev. Process. Ind.* **2007**, *20*, 158–164. [CrossRef]
8. Hussein, H.; Brennan, S.; Molkov, V. Hydrogen Jet Fire from a Thermally Activated Pressure Relief Device (TPRD) from Onboard Storage in a Naturally Ventilated Covered Car Park. *Hydrogen* **2021**, *2*, 343–361. [CrossRef]
9. Moradi, R.; Groth, K.M. Hydrogen storage and delivery: Review of the state of the art technologies and risk and reliability analysis. *Int. J. Hydrogen Energy* **2019**, *44*, 12254–12269. [CrossRef]
10. Abohamzeh, E.; Salehi, F.; Sheikholeslami, M.; Abbassi, R.; Khan, F. Review of hydrogen safety during storage, transmission, and applications processes. *J. Loss Prev. Process. Ind.* **2021**, *72*, 104569. [CrossRef]
11. Zhang, R.; Fujimori, S.; Dai, H.; Hanaoka, T. Contribution of the transport sector to climate change mitigation: Insights from a global passenger transport model coupled with a computable general equilibrium model. *Appl. Energy* **2018**, *211*, 76–88. [CrossRef]
12. Middha, P.; Hansen, O.R. Using computational fluid dynamics as a tool for hydrogen safety studies. *J. Loss Prev. Process. Ind.* **2009**, *22*, 295–302. [CrossRef]
13. Wu, Y. Assessment of the impact of jet flame hazard from hydrogen cars in road tunnels. *Transp. Res. Part C Emerg. Technol.* **2008**, *16*, 246–254. [CrossRef]

14. Seike, M.; Kawabata, N.; Hasegawa, M.; Tanaka, H. Heat release rate and thermal fume behavior estimation of fuel cell vehicles in tunnel fires. *Int. J. Hydrogen Energy* **2019**, *44*, 26597–26608. [CrossRef]
15. Shibani; Salehi, F.; Baalisampang, T.; Abbassi, R. Numerical modeling towards the safety assessment of multiple hydrogen fires in confined areas. *Process. Saf. Environ. Prot.* **2022**, *160*, 594–609. [CrossRef]
16. LaFleur, C.B.; Anleu, G.A.B.; Muna, A.B.; Ehrhart, B.D.; Blaylock, M.L.; Houf, W.G. *Hydrogen Fuel Cell Electric Vehicle Tunnel Safety Study*; Sandia National Lab: Livermore, CA, USA, 2017. [CrossRef]
17. Schefer, R.; Houf, W.; Williams, T.; Bourne, B.; Colton, J. Characterization of high-pressure, underexpanded hydrogen-jet flames. *Int. J. Hydrogen Energy* **2007**, *32*, 2081–2093. [CrossRef]
18. Schefer, R.; Merilo, E.; Groethe, M.; Houf, W. Experimental investigation of hydrogen jet fire mitigation by barrier walls. *Int. J. Hydrogen Energy* **2011**, *36*, 2530–2537. [CrossRef]
19. Baalisampang, T.; Abbassi, R.; Garaniya, V.; Khan, F.; Dadashzadeh, M. Fire impact assessment in FLNG processing facilities using Computational Fluid Dynamics (CFD). *Fire Saf. J.* **2017**, *92*, 42–52. [CrossRef]
20. Hansen, O.R. Hydrogen infrastructure—Efficient risk assessment and design optimization approach to ensure safe and practical solutions. *Process. Saf. Environ. Prot.* **2020**, *143*, 164–176. [CrossRef]
21. Iñaki, A.A.; Buttner, W.; Barthélémy, H.; Cirrone, D.; Coldrick, S.; Hooker, P.; Hawksworth, S.; Jeffrey, K.; Jordan, T.; Keller, J.; et al. *International Association for Hydrogen Safety 'Research Priorities Workshop'*; HSE: Buxton, UK, 2018.
22. Liu, Q.; Xu, Z.; Xu, W.; Tagne, S.M.S.; Tao, H.; Zhao, J.; Ying, H. Study of the Heat Exhaust Coefficient of Lateral Smoke Exhaust in Tunnel Fires: The Effect of Tunnel Width and Transverse Position of the Fire Source. *Fire* **2022**, *5*, 167. [CrossRef]
23. Hu, L.; Chen, L.; Wu, L.; Li, Y.; Zhang, J.; Meng, N. An experimental investigation and correlation on buoyant gas temperature below ceiling in a slopping tunnel fire. *Appl. Therm. Eng.* **2013**, *51*, 246–254. [CrossRef]
24. Li, Y.; Xiao, J.; Zhang, H.; Breitung, W.; Travis, J.; Kuznetsov, M.; Jordan, T. Numerical analysis of hydrogen release, dispersion and combustion in a tunnel with fuel cell vehicles using all-speed CFD code GASFLOW-MPI. *Int. J. Hydrogen Energy* **2021**, *46*, 12474–12486. [CrossRef]
25. Li, J.; Tian, Y.; Li, Y.; Zhao, Y.; Huang, Y. Numerical and Experimental Study on the Effects of the Slope on the Critical Velocity in Titled Tunnels. *Procedia Eng.* **2017**, *205*, 1864–1870. [CrossRef]
26. Salvetti, I.M.V.; Meyers, B.J.; Sagaut, F.P. *Quality and Reliabilty of Large-Eddy Simulations II*; Springer Science: Cham, Switzerland, 2011; Volume 16.
27. Pope, S.B. *Turublent Flows*; Cambridge University Press: Cambridge, UK, 2001.
28. Thierry Poinsot, D.V. Theoretical and Numerical Combustion, Second Edition. *Decis. Support Syst.* **2005**, *38*, 557–573.
29. Mohammadfam, I.; Zarei, E. Safety risk modeling and major accidents analysis of hydrogen and natural gas releases: A comprehensive risk analysis framework. *Int. J. Hydrogen Energy* **2015**, *40*, 13653–13663. [CrossRef]
30. Marc, J.A.; Konstantinos, E.K. *Fires, Explosions, and Toxic Gas Dispersions. Effects Calculation and Risk Analysis*; Taylor and Francis Group: Oxford, UK, 2010.
31. Marchi, C.S.; Hecht, E.; Ekoto, I.; Groth, K.; LaFleur, C.; Somerday, B.; Mukundan, R.; Rockward, T.; Keller, J.; James, C. Overview of the DOE hydrogen safety, codes and standards program, part 3: Advances in research and development to enhance the scientific basis for hydrogen regulations, codes and standards. *Int. J. Hydrogen Energy* **2017**, *42*, 7263–7274. [CrossRef]
32. Wu, Y.; Bakar, M. Control of smoke flow in tunnel fires using longitudinal ventilation systems—A study of the critical velocity. *Fire Saf. J.* **2000**, *35*, 363–390. [CrossRef]
33. Mashhadimoslem, H.; Ghaemi, A.; Palacios, A.; Behroozi, A.H. A new method for comparison thermal radiation on large-scale hydrogen and propane jet fires based on experimental and computational studies. *Fuel* **2020**, *282*, 118864. [CrossRef]